AFRL-RV-PS-
TR-2013-0073

SPACECRAFT DEBRIS AVOIDANCE USING POSITIVELY INVARIANT CONSTRAINT ADMISSIBLE SETS

Ilya Vladimir

Regents Of The University Of Michigan
Division Of Research, Development And Administration
503 Thompson St
Ann Arbor, MI 48109-1340

11 Jul 2013

Final Report

AIR FORCE RESEARCH LABORATORY
Space Vehicles Directorate
3550 Aberdeen Ave SE
AIR FORCE MATERIEL COMMAND
KIRTLAND AIR FORCE BASE, NM 87117-5776

DTIC COPY
NOTICE AND SIGNATURE PAGE

This report is the result of contracted fundamental research deemed exempt from public affairs security and policy review in accordance with SAF/AQR memorandum dated 10 Dec 08 and AFRL/CA policy clarification memorandum dated 16 Jan 09. This report is available to the general public, including foreign nationals. Copies may be obtained from the Defense Technical Information Center (DTIC) (http://www.dtic.mil).

AFRL-RV-PS-TR-2013-0073 HAS BEEN REVIEWED AND IS APPROVED FOR PUBLICATION IN ACCORDANCE WITH ASSIGNED DISTRIBUTION STATEMENT

//SIGNED//
MORGAN BALDWIN
Program Manager

//SIGNED//
PAUL HAUSGEN
Technical Advisor, Spacecraft Component Technology Branch

//SIGNED//
CHRISTOPHER D. STOIK, Lt Col, USAF
Deputy Chief, Spacecraft Technology Division
Space Vehicles Directorate

REPORT DOCUMENTATION PAGE

Form Approved
OMB No. 0704-0188

1. REPORT DATE *(DD-MM-YYYY)*	2. REPORT TYPE	3. DATES COVERED *(From - To)*
11-07-2013	Final Report	22 Nov 2011 – 21 May 2013

4. TITLE AND SUBTITLE

Spacecraft Debris Avoidance Using Positively Invariant Constraint Admissible Sets

5a. CONTRACT NUMBER
FA9453-12-1-0134

5b. GRANT NUMBER

5c. PROGRAM ELEMENT NUMBER
61102F

6. AUTHOR(S)

Ilya Vladimir

5d. PROJECT NUMBER
2304

5e. TASK NUMBER
PPM00011766

5f. WORK UNIT NUMBER
EF007890

7. PERFORMING ORGANIZATION NAME(S) AND ADDRESS(ES)

Regents Of The University Of Michigan
Division Of Research, Development and Administration
503 Thompson St
Ann Arbor, MI 48109-1340

8. PERFORMING ORGANIZATION REPORT

9. SPONSORING / MONITORING AGENCY NAME(S) AND ADDRESS(ES)

Air Force Research Laboratory
Space Vehicles Directorate
3550 Aberdeen Ave. SE
Kirtland AFB, NM 87117-5776

10. SPONSOR/MONITOR'S ACRONYM(S)
AFRL/RVSV

11. SPONSOR/MONITOR'S REPORT NUMBER(S)
AFRL-RV-PS-TR-2013-0073

12. DISTRIBUTION / AVAILABILITY STATEMENT

Approved for public release; distribution is unlimited.

13. SUPPLEMENTARY NOTES

14. ABSTRACT

This technology described a technique for spacecraft maneuver planning that uses positively-invariant sets in order to avoid collisions with debris, while adhering to specified thrust limits. The approach is based on hopping between neighborhoods of equilibria in a virtual net, and maintaining the spacecraft trajectory within a tube formed by safe positively-invariant sets. For the case where thrust limits can be specified as polyhedral norm bounds, we have shown that the thrust limit on the growth distance can be easily computed; it is, in fact, feasible to perform these computations onboard a spacecraft in order to account for thruster failure or degradation. We described an extension in the presence of moving debris using contractive constraint admissible sets in order to avoid collisions. Lastly, we illustrated that the approach can be extended to include unmeasured bounded disturbances.

15. SUBJECT TERMS Debris Representation; Static Debris Avoidance Approach; Growth Distance Computations; Connectivity Graph; Graph Search; Bounded Disturbances; Linear Time-Varying (LTV); Clohessy-Wiltshire-Hill (CWH)

16. SECURITY CLASSIFICATION OF:			17. LIMITATION OF ABSTRACT	18. NUMBER OF PAGES	19a. NAME OF RESPONSIBLE PERSON
					Morgan Baldwin
a. REPORT	b. ABSTRACT	c. THIS PAGE	Unlimited	44	19b. TELEPHONE NUMBER *(include area code)*
Unclassified	Unclassified	Unclassified			

(This page intentionally left blank)

TABLE OF CONTENTS

LIST OF FIGURES

LIST OF TABLES

ACKNOWLEDGMENTS AND DISCLAIMER

Acknowledgement

This material is based on research sponsored by Air Force Research Laboratory under agreement number FA9453-12-1-0134. The U.S. Government is authorized to reproduce and distribute reprints for Governmental purposes notwithstanding any copyright notation thereon.

Disclaimer

The views and conclusions contained herein are those of the authors and should not be interpreted as necessarily representing the official policies or endorsements, either expressed or implied, of Air Force Research Laboratory or the U.S. Government.

1 SUMMARY

Contributions of this research are the development of an on-board relative motion maneuver planning approach for spacecraft debris avoidance that can handle set bounded disturbances. In this report we describe the development of an on-board maneuver planning approach based on the use of constraint-admissible positively invariant sets [1]. The sets determine connectivity between forced and unforced spacecraft equilibria in the Clohessy-Wiltshire-Hill (CWH) relative motion frame [2]. The collection of equilibria form a *virtual net* in the vicinity of the spacecraft. Two equilibria are connected if a choice of a Linear Quadratic (LQ) feedback gain can be made that results in a transition between the equilibria which avoids collision with a potentially moving debris/obstacle while satisfying limits on thrust. A connectivity graph for all the equilibria in the net is constructed based on *fast growth distance* computation between two ellipsoidal sets, while real-time graph search algorithms are used to optimize an equilibria hopping sequence to avoid debris collisions. Unlike existing spacecraft trajectory optimization techniques, our method does not rely on precise assignment of spacecraft position along the trajectory, and is able to assure robustness to unmeasured (but set-bounded) disturbances and uncertainties.

The following papers have been published related to the subject matter of this report.

- A. Weiss, M. Baldwin, R. S. Erwin, and I. Kolmanovsky, "Spacecraft Constrained Maneuver Planning for Moving Obstacle Avoidance Using Positively Invariant Constraint Admissible Sets," *Proc. Amer. Contr. Conf.*, Washington, DC, June 2013.

- A. Weiss, M. Baldwin, R. S. Erwin, and I. Kolmanovsky, "Spacecraft Constrained Maneuver Planning Using Positively Invariant Constraint Admissible Sets," *Bar-Itzhack Memorial Symposium*, Haifa, Israel, October 2012.

- M. Baldwin, A. Weiss, I. Kolmanovsky, and R. S. Erwin, "Spacecraft Debris Avoidance using Positively Invariant Constraint Admissible Sets," *AAS/AIAA Space Flight Mechanics Meeting*, Charleston, SC, January 2012, AAS-12-250 .

The project has supported one doctoral student (Avishai Weiss) for one year of his doctoral studies.

2 INTRODUCTION

Orbital debris is a growing problem, with about 40% of ground-trackable objects originating from explosions that now number approximately 5 per year [3]. Spacecraft maneuver planning procedures thus have to address debris avoidance requirements. While obstacle avoidance is a standard problem in robotics [4, 5], the related spacecraft problems have several unique features. In particular, the space environment is relatively uncluttered, thus permitting for a variety of maneuvers. Spacecraft dynamics are quite different from those of typical robots. Maneuver efficiency with

respect to time and fuel consumption is a critical consideration. The states of the spacecraft and the debris can only be estimated, often with a significant estimation error. Finally, computational algorithms must be fast and optimized given moving objects and the limited computing power onboard most spacecraft. These unique features of spacecraft maneuver planning problems provide the motivation for the development of specialized algorithms.

Interest in spacecraft trajectory optimization with obstacle avoidance has increased in recent years. An optimal control problem with path constraints constructed as 'keep out' zones to avoid obstacles was formulated in [6]. The Sparse Optimal Control Software (SOCS) software was then used to solve the problem [7]. Another nonlinear optimal control formulation was used in [8] to solve for minimum-fuel rendezvous between a target and chaser, where collision avoidance requirements were incorporated as inequality constraints. The method involved solving a sequence of unconstrained optimal control problems, whose solution converges to the solution of the original problem. A 3-D static optimization over final relative position and time-of-flight such that obstacles are avoided and cost is optimized is presented in [9]. Feedback is incorporated by re-planning over either constant or variable time intervals.

Debris avoidance strategies have also been defined utilizing collision avoidance probabilities. Collision avoidance strategies based upon the number of evasive maneuvers, expected risk reduction, false alarm rate, required propellant consumption, and mass fraction for an accepted collision probability are presented in [10].

Guidance based on artificial potential function is used in [9, 11] to determine a rendezvous path free of obstacles. A potential function is developed with the intent that a minimum occurs at a desired relative position and then a dynamic control law is used to ensure the trajectory is obstacle free [11].

The spacecraft obstacle avoidance problem has also been treated using linear programming techniques [12–15]. In [12], the minimum-fuel avoidance maneuver is formulated with linear constraints and discrete dynamics modeled as an linear time-varying (LTV) system. In [13], the trajectory optimization problem is formulated as a linear programming problem with the capability of including operational constraints and the optimal number of maneuvers is determined. In [14], a mixed-integer linear program results from combining collision avoidance, trajectory optimization, and fleet assignment to obtain the optimal solution for spacecraft maneuvers. A robust linear programming technique is proposed in [15]. The maneuver can be constructed by solving a linear programming problem with no integer constraints and guaranteeing collision avoidance with respect to bounded navigation uncertainty.

3 METHODS, ASSUMPTIONS, AND PROCEDURES

We develop a chained invariant set method to avoid both static and moving debris during spacecraft relative motion maneuvers. The equations of motion for spacecraft orbital dynamics are reviewed in Appendix A. We use linearized equations of motion (A.3), where continuous thrust actuation $U_k = [F_{x,k},\ F_{y,k},\ F_{z,k}]^{\mathrm{T}}$ is assumed.

Our approach to debris avoidance is based on utilizing constraint-admissible positively invariant sets [1, 16–18] centered around spacecraft forced and unforced equilibria. A finite set of these equilibria used for constructing debris avoidance maneuvers is referred to as a *virtual net.* Given an estimate of the debris position, we build a connectivity graph that identifies the equilibria in the virtual net between which the spacecraft can move, with guaranteed collision-free motion and within the available thrust authority. We then employ graph search to determine an efficient path between the equilibria that ensures debris avoidance. One of the main reasons this framework is attractive compared to alternatives such as open-loop trajectory planning, is the ability to incorporate bounded disturbances such as thrust errors, air drag, and solar pressure.

3.1 Virtual Net

The virtual net comprises a finite set of equilibria, $X_e(r)$, corresponding to a finite set of prescribed spacecraft positions $r \in \mathcal{N} = \{r_1, r_2, \ldots, r_n\} \subset R^3$,

$$X_e(r_k) = \begin{bmatrix} r_k & 0 \end{bmatrix}^{\mathrm{T}} = \begin{bmatrix} r_{x,k} & r_{y,k} & r_{z,k} & 0 & 0 & 0 \end{bmatrix}^{\mathrm{T}}, \quad k = 1, \cdots, n, \tag{1}$$

whose velocity states are zero, and where n is the number of equilibria in the virtual net. See Figure 1. We assume that for all $r \in \mathcal{N}$, the corresponding values of control necessary to support the specified equilibria in steady-state satisfy the imposed thrust limits.

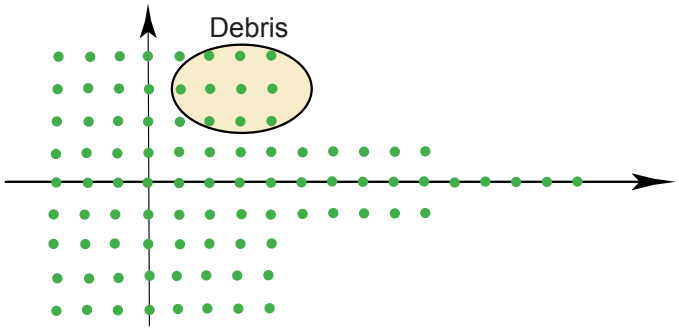

Figure 1: The virtual net for debris avoidance. Dots correspond to positions at equilibria, $X_e(r)$, on a virtual net. The ellipsoid represents the debris position and uncertainty.

3.2 LQ Controller with Gain Switching

A conventional Linear-Quadratic (LQ) feedback

$$U = K(X - X_e(r)) + \Gamma r = KX + H(K)r, \tag{2}$$

is used to control the spacecraft thrust to arrive at a commanded equilibrium (1), where

$$\Gamma = \begin{bmatrix} -3n^2 m_c & 0 & 0 \\ 0 & 0 & 0 \\ 0 & 0 & n^2 m_c \end{bmatrix},$$

$$H(K) = \Gamma - K \begin{bmatrix} I_3 \\ 0_3 \end{bmatrix},$$

and where I_3 denotes the 3×3 identity matrix while 0_3 denotes the 3×3 zero matrix. The LQ controller provides an asymptotically stable closed-loop system but does not enforce debris avoidance constraints.

To provide greater flexibility in handling constraints, a multimode controller architecture is employed [16]. Specifically, we assume that a finite set of LQ gains $K \in \mathcal{K} = \{K_1, \cdots, K_m\}$ is available to control the spacecraft. By using a large control weight in the LQ cost functional, motions with low fuel consumption yet large excursions can be generated; using a large control weight in the LQ cost, motions with short transition time can be generated [19]. We assume that a preference ordering has been defined and the gains are arranged in the order of descending preference, from K_1 being the highest preference gain to K_m being the lowest preference gain.

3.3 Positively Invariant Sets

The ellipsoidal set

$$\bar{C}(r,K) = \{X \in R^6 : \frac{1}{2}(X - X_e(r))^T P(K)(X - X_e(r)) \leq 1\} \subset R^6, \tag{3}$$

where

$$\bar{A}(K)^{\mathrm{T}} P \bar{A}(K) - P < 0, \tag{4}$$

$\bar{A}(K) = (A + BK)$, and $P = P(K) > 0$ is positively invariant for the closed-loop dynamics. Positive invariance implies that any trajectory of the closed-loop system that starts in $\bar{C}(r,K)$ is guaranteed to stay in $\bar{C}(r,K)$ as long as the same LQ gain K is used and the set-point command r is maintained. To achieve the positive invariance, the matrix P can be obtained as the solution of the discrete-time Riccati equation in the LQ problem or as the solution of the above Lyapunov equation for the closed-loop asymptotically stable system. We note that, because the system is linear, the positive invariance of $\bar{C}(r,K)$ implies the positive invariance of the scaled set

$$C(r,K,\rho) = \{X \in R^6 : \frac{1}{2}(X - X_e(r))^T P(K)(X - X_e(r)) \leq \rho^2\}, \quad \rho \geq 0.$$

Geometrically, the set $C(r,K,\rho)$ corresponds to an ellipsoid scaled by the value of ρ and centered around $X_e(r)$, $r \in \mathcal{N}$.

3.4 Debris Representation

We use a set, $O(z,Q)$, centered around the position $z \in R^3$, to over-bound the position of the debris, i.e.,

$$O(z,Q) = \{X \in R^6 : (SX - z)^T Q(SX - z) \leq 1\}, \tag{5}$$

where $Q = Q^{\mathrm{T}} > 0$ and

$$S = \begin{bmatrix} 1 & 0 & 0 & 0 & 0 & 0 \\ 0 & 1 & 0 & 0 & 0 & 0 \\ 0 & 0 & 1 & 0 & 0 & 0 \end{bmatrix}. \tag{6}$$

The set $O(z,Q)$ can account for the debris and spacecraft physical sizes and also for the uncertainties in the estimation of the debris/spacecraft position. Note that the set $O(z,Q)$ has an ellipsoidal shape in the position directions and it is unbounded in the velocity directions. Ellipsoidal sets, rather than polyhedral sets, are used here to over-bound the debris, since ellipsoidal bounds are typically produced by position estimation algorithms, such as the Extended Kalman Filter (EKF).

3.5 Static Debris Avoidance Approach

Consider now $r_i \in \mathcal{N}$, representing a possible position on the net that the spacecraft can move to as a part of the debris avoidance maneuver. Suppose that the current state of the spacecraft is $X(t_0)$ at the time instant $t_0 \in Z^+$. If there exists a $\rho \geq 0$ and $K_j \in \mathcal{K}$ such that

$$X(t_0) \in C(r_i,K_j,\rho) \text{ and } O(z,Q) \cap C(r_i,K_j,\rho) = \emptyset, \tag{7}$$

the spacecraft can move to the position $r_i \in \mathcal{N}$ by engaging the control law with $r(t) = r_i$ and $K(t) = K_j$, $t \geq t_0$, and without hitting the debris confined to $O(z,Q)$. This idea underlies our subsequent approach to debris avoidance, where we maintain the spacecraft within a tube formed by positively invariant sets that do not intersect with debris.

The minimum value of $\rho \geq 0$ for which $O(z,Q) \bigcap C(r,K,\rho) \neq \emptyset$ is referred to as the *growth distance* [20]. This growth distance can also be viewed as the least upper bound on the values of ρ for which $O(z,Q)$ and $C(r,K,\rho)$ do not intersect. See Figure 2. We use the notation $\rho_g(r,K,Q,z)$ to reflect the dependence of the growth distance on the set-point $r \in \mathcal{N}$, the control gain $K \in \mathcal{K}$ and the obstacle parameters Q and z.

Note that the growth distance depends on the position of the debris which may be unknown in advance. Consequently, growth distance computations have to be performed online.

Since spacecraft have limited thrust, we additionally define a maximum value of $\rho = \rho_u(r,K)$ for which $X \in C(r,K,\rho_u(r,K))$ implies that the thrust $U = KX + H(K)r$ satisfies the imposed thrust limits. We refer to ρ_u as the *thrust limit on growth distance.* Unlike ρ_g, the value of ρ_u does not

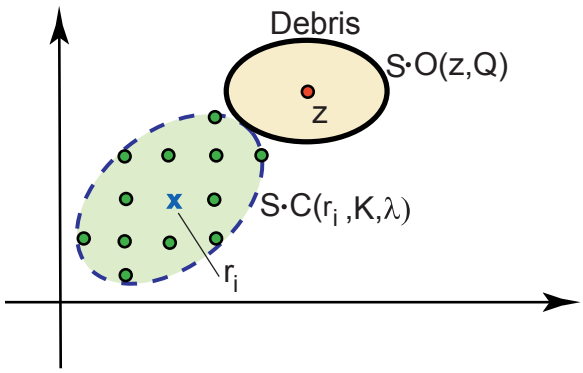

Figure 2: The positively invariant set is grown till it touches the debris.

depend on the position or shape of the debris and can be pre-computed off-line.

Finally, we define *the thrust limited growth distance*

$$\rho^*(r,K,Q,z) = \min\{\rho_g(r,K,Q,z),\rho_u(r,K)\}. \tag{8}$$

Note that $X(t_0) \in C(r_i,K_j,\rho^*(r_i,K_j,z))$ implies that the ensuing closed-loop spacecraft trajectory under the control (2), where $r(t) = r_i$ and $K(t) = K_j$ for $t \geq t_0$, satisfies the thrust limits and avoids collisions with a debris confined to $O(z,Q)$.

The above definitions were given for the case of a single stationary debris, $O(z,Q)$. In the case of multiple debris, the growth distance is replaced by the *multi-growth distance*, which is the minimum growth distance to each of $O(z_l,Q_l)$, $l = 1,\cdots,n_d$.

3.6 Growth Distance Computations

Define $\bar{X} = X - X_e(r)$ and $\alpha = 2\rho^2$. The problem of determining the growth distance $\rho_g(r,K,Q,z)$, reduces to the following constrained optimization problem:

$$\begin{array}{ll} \min\limits_{\alpha,\bar{X}} & \alpha \\ \text{subject to} & \bar{X}^{\mathrm{T}}P\bar{X} \leq \alpha \\ & ((S(\bar{X}+X_e(r))-z)^{\mathrm{T}}Q((S(\bar{X}+X_e(r))-z) \leq 1 \end{array} \tag{9}$$

To solve this optimization problem, we use the Karush-Kuhn-Tucker (KKT) conditions [21,22]. Note that standard linear independence constraint qualification conditions hold given that $P > 0$. We define

$$\mathcal{L} = \alpha + \lambda_1(\bar{X}^{\mathrm{T}}P\bar{X} - \alpha) + \lambda_2((S(\bar{X}+X_e(r))-z)^{\mathrm{T}}Q(S(\bar{X}+X_e(r))-z) - 1),$$

where λ_1 and λ_2 are Lagrange multipliers. The stationarity of the Lagrangian (setting partial derivative equal to zero) with respect to α yields $\lambda_1 = 1$. The stationarity of the Lagrangian with respect to $\bar{X}$ yields

$$\bar{X} = \bar{X}(\lambda_2, r, z) = -(P + \lambda_2 S^{\mathrm{T}} Q S)^{-1} S^{\mathrm{T}} Q (S X_e(r) - z)\lambda_2, \tag{10}$$

where the scalar $\lambda_2 \geq 0$ is to be determined. Note that $P > 0$, $S^{\mathrm{T}} Q S \geq 0$, $\lambda_2 \geq 0$ (as the Lagrange multiplier corresponding to an inequality constraint) imply that $(P + \lambda_2 S^{\mathrm{T}} Q S)$ is invertible. The problem reduces to finding a nonnegative scalar λ_2, which is the root of

$$F(\lambda_2, r, z) = ((S X - z)^{\mathrm{T}} Q (S X - z) - 1 = 0, \tag{11}$$

where

$$X = \bar{X}(\lambda_2, r, z) + X_e(r).$$

The scalar root finding problem (11) has to be solved online multiple times for different $r \in \mathcal{N}$, and in the case of avoiding a predicted debris path also for different z's. To solve this problem fast, while reusing previously found solutions as approximations, a dynamic Newton-Raphson's algorithm is used [22–24]. This algorithm uses predictor-corrector updates to track the root as a function of z and r, and is given by

$$\begin{aligned}
\lambda_2^{k+1,+} &= \lambda_2^k + \{\frac{\partial F}{\partial \lambda_2}(\lambda_2^k, z^k, r^k)\}^{-1}\{-F(\lambda_2^k, z^k, r^k) - \frac{\partial F}{\partial z}(\lambda_2^k, z^k, r^k)(z^{k+1} - z^k) \\
&\quad - \frac{\partial F}{\partial r}(\lambda_2^k, z^k, r^k)(r^{k+1} - r^k)\}, \\
\lambda_2^{k+1} &= max\{0, \lambda_2^{k+1,+}\}.
\end{aligned}$$

To implement the algorithm, we take advantage of the known functional form for F and explic-

itly compute the partial derivatives,

$$\begin{aligned}
\frac{\partial \bar{X}}{\partial \lambda_2} &= (P + \lambda_2 S^{\mathrm{T}} Q S)^{-1} \left\{ -S^{\mathrm{T}} Q (S X_e(r) - z) - S^{\mathrm{T}} Q S \bar{X} \right\}, \\
\frac{\partial F}{\partial \lambda_2} &= 2(S X - z)^{\mathrm{T}} Q (S \frac{\partial \bar{X}}{\partial \lambda_2}), \\
\frac{\partial \bar{X}}{\partial r} &= (P + \lambda_2 S^{\mathrm{T}} Q S)^{-1} \left\{ -S^{\mathrm{T}} Q S \Omega \right\} \lambda_2, \\
\frac{\partial F}{\partial r} &= 2(S \bar{X} - z + r)^{\mathrm{T}} Q (S \frac{\partial \bar{X}}{\partial r} + I_3), \\
\frac{\partial \bar{X}}{\partial z} &= (P + \lambda_2 S^{\mathrm{T}} Q S)^{-1} S^{\mathrm{T}} Q S \Omega \lambda_2, \\
\frac{\partial F}{\partial z} &= 2(S \bar{X} - z + r)^{\mathrm{T}} Q (S \frac{\partial \bar{X}}{\partial z} - I_3),
\end{aligned} \tag{12}$$

where, $X_e(r) = \Omega r$,

$$\Omega = \begin{bmatrix} I_3 \\ 0 \end{bmatrix},$$

and I_3 denotes the 3×3 identity matrix. Note that $S\Omega = I_3$.

Figure 3 illustrates growth distance tracking. For the first 20 iterations, r^k is held constant to enable initial convergence of the algorithm. Then, r^k varies through the virtual net. One iteration of the Newton-Raphson algorithm per value of r^k is used to update the root, λ_2^{k+1}. Figure 3b demonstrates that the growth distance tracking is accurate. The growth distance is occasionally zero indicating an overlap between several r^k and the debris. Figure 3c illustrates the trajectory of r^k in three dimensions.

3.7 Thrust Limit on Growth Distance Computations

Suppose that the thrust limits are expressed in the form $\|LU\| \leq 1$ for an appropriately defined matrix L and norm $\|\cdot\|$. The computational procedures to determine $\rho_u(r, K)$ involve solving a bilevel optimization problem where $\|L(KX + H(K)r)\|$ is maximized subject to the constraint $X \in C(r, K, \alpha)$, and bisections are performed on the value of α so that the maximum value is driven to 1. As we demonstrate in this section, in special cases this computation can be greatly simplified.

Suppose that the thrust constraints are prescribed in terms of polyhedral norm bounds, specifically

$$e_i^{\mathrm{T}}(KX + Hr) \leq u_{\max}, \quad i = 1, 2, \cdots, m, \tag{13}$$

where e_i are the vertices of the unit norm polytope, and $u_{\max}$ is the norm bound. The infinity norm,

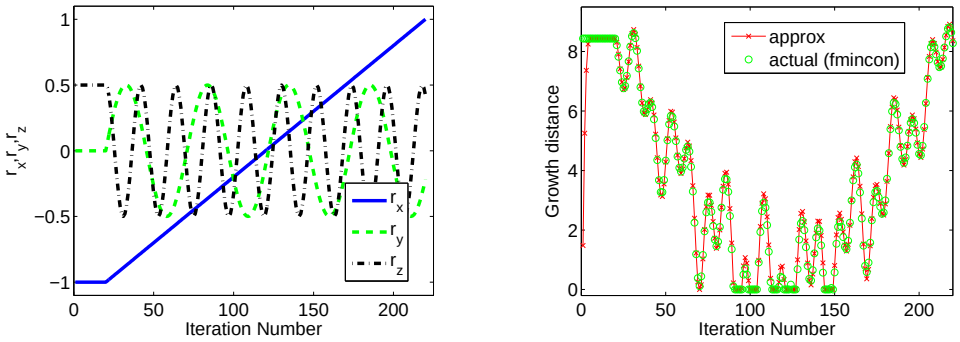

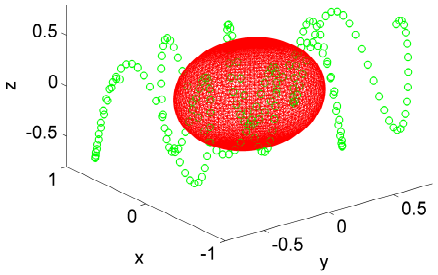

Figure 3: (a) Components of r, varying versus iteration number. (b) Growth distance versus iteration number computed by Newton-Raphson algorithm. (c) The trajectory of r and the debris.

for instance, has $m = 6$, and

$$e_1 = \begin{bmatrix} 1 \\ 0 \\ 0 \end{bmatrix} \quad e_2 = \begin{bmatrix} -1 \\ 0 \\ 0 \end{bmatrix} \quad e_3 = \begin{bmatrix} 0 \\ 1 \\ 0 \end{bmatrix}$$
$$e_4 = \begin{bmatrix} 0 \\ -1 \\ 0 \end{bmatrix} \quad e_5 = \begin{bmatrix} 0 \\ 0 \\ 1 \end{bmatrix} \quad e_6 = \begin{bmatrix} 0 \\ 0 \\ -1 \end{bmatrix}. \tag{14}$$

In the case of non-polyhedral norm bounds, such as the 2-norm, an approximation by a polyhedral norm bound may be employed.

The thrust limit on the growth distance is then determined based on solving, for $i = 1, \cdots, n$, the

optimization problems

$$\begin{array}{ll} \text{maximize} & e_i^{\mathrm{T}}(KX + Hr) \\ \text{subject to} & \frac{1}{2}(X - X_e(r))^{\mathrm{T}} P (X - X_e(r)) \leq c. \end{array} \tag{15}$$

If the value of c is found for which the solutions X_i^* of (15) satisfy $\max_i\{e_i^{\mathrm{T}}(KX_i^* + Hr)\} = u_{\max}$, then $\rho_u(r, K) = \sqrt{c}$.

The problem (15) can be solved by diagonalizing P, using an orthogonal matrix, V,

$$P = V^{\mathrm{T}} \Lambda V, \; \Lambda = \mathrm{diag}[\lambda_1^2, \cdots, \lambda_6^2], \lambda_i > 0.$$

By defining, $z = X - X_e(r)$, and ζ so that

$$z = V^{\mathrm{T}} \Lambda^{-\frac{1}{2}} \zeta,$$

it follows that

$$\begin{array}{rcl} z^{\mathrm{T}} P z & = & \zeta^{\mathrm{T}} \Lambda^{-\frac{1}{2}} V P V^{\mathrm{T}} \Lambda^{-\frac{1}{2}} \zeta \\ & = & \zeta^{\mathrm{T}} \zeta. \end{array}$$

The problem (15) can now be re-written as

$$\begin{array}{ll} \text{maximize} & h_i^{\mathrm{T}} \zeta + e_i^{\mathrm{T}} \Gamma r \\ \text{subject to} & \frac{1}{2} \zeta^{\mathrm{T}} \zeta \leq c, \end{array} \tag{16}$$

where

$$h_i^{\mathrm{T}} = e_i^{\mathrm{T}} K V^{\mathrm{T}} \Lambda^{-\frac{1}{2}}.$$

The solution to the constrained maximization problem (16) of maximizing the inner-product of two vectors over a unit 2-norm ball is given by

$$\zeta_i = \frac{h_i}{||h_i||} \sqrt{2c}, \tag{17}$$

where $||\cdot||$ denotes the vector 2-norm. The maximum value of the objective function in (15) is given by

$$||h_i|| \sqrt{2c} + e_i^{\mathrm{T}} \Gamma r.$$

Consequently, to satisfy (13), we let

$$c = \begin{cases} 0, & \text{if } \exists\, i : u_{\max} \leq e_i^{\mathrm{T}} \Gamma r, \\ \min\limits_i \dfrac{1}{2} \left(\dfrac{u_{\max} - e_i^{\mathrm{T}} \Gamma r}{||h_i||} \right)^2, & \text{otherwise.} \end{cases} \tag{18}$$

Thus, the problem of finding the thrust limit on the growth distance for polyhedral norm bounds has an explicit solution given by (18). Even though the computation of thrust limits on the growth distance can be performed offline for the nominal operating conditions, fast computational procedures are beneficial in case of thruster failures, degradations, and restrictions on thrust directions (e.g., caused by the presence of other spacecraft nearby), all of which can lead to changing constraints on thrust during spacecraft missions.

We note that the condition $u_{\max} \geq \max_i\{e_i^{\mathrm{T}}\Gamma r\}$ is satisfied if the available thrust can maintain the equilibrium $X_e(r)$ in steady-state. We also note, that, based on the form of Γ, c is independent of r_y, the in-track component of the equilibrium in the virtual net. Hence the computations of $\rho_u(r, K)$ need only be performed with $r_y = 0$.

When a spacecraft does not have independent thrusters in x, y and z directions, a 2-norm thrust limit is more practical. Unfortunately, (15) is, in general, a non-convex problem. In this case, the 2-norm bound can be approximated by a polyhedral norm bound (13), with the vertices e_i selected on the unit 2-norm ball in R^3. We note that higher accuracy of this approximation requires a higher number of vertices in (13), which thus, complicates (18).

Finally, we note that when Δv's are treated as control inputs, the thrust limit on growth distance is induced by the available Δv. In this case, computing the thrust limited growth distance is completely analogous to computing it in the case when the control input is the thrust force or thrust acceleration.

3.8 Connectivity Graph and Graph Search

We now introduce a notion of *connectivity* between two vertices of the virtual net, $r_i \in \mathcal{N}$ and $r_j \in \mathcal{N}$. The vertex r_i is connected to the vertex r_j if there exists a gain $K \in \mathcal{K}$ such that

$$X_e(r_i) \in int\, C(r_j, K, \rho^*(r_j, K, z)), \tag{19}$$

where *int* denotes the interior of a set. The connectivity implies that a spacecraft located close to an equilibrium corresponding to r_i can transition to an equilibrium $X_e(r_j)$ by using limited thrust and avoiding collision with the debris. We note that if r_i is connected to r_j this does not imply that, in turn, r_j is connected to r_i. We also note that connectivity depends on the existence of an appropriate control gain from the set of gains $\mathcal{K}$ but the condition (19) does not need to hold for all gains.

The on-line motion planning with debris avoidance is performed according to the following procedure (for simplicity, described here for the case of a single debris):

Step 1: Determine the debris location and shape (i.e., z and Q).

Step 2: By using fast growth distance computations, determine the thrust limited growth distance based on (8), with ρ_g computed online and ρ_u precomputed offline.

Step 3: Construct a graph connectivity matrix between all $r_i, r_j \in \mathcal{N}$. In the graph connectivity matrix, if two vertices are not connected, the corresponding matrix element is zero; if they are connected the corresponding matrix element is 1. In parallel, build the control gain selectivity matrix, which identifies the index of the highest preference gain K for which r_i and r_j are connected. This gain will be applied if the edge connecting r_i and r_j is traversed.

Step 4: Perform graph search to determine a sequence of connected vertices $r[k] \in \mathcal{N}$ and control gains $K[k] \in \mathcal{K}$, $k = 1, \cdots, l_p$, such that $r[1]$ satisfies the initial constraints, $r[l_p]$ satisfies the final constraints, and the path length l_p is minimized.

Per the above algorithm, graph search is utilized to determine the minimum number of equilibrium hops around a piece of debris. After the path has been determined as a sequence of the set-points and the corresponding control gains, the execution of the path proceeds by checking if the current state, $X(t)$ is in the safe positively invariant set corresponding to the next reference r^+ and next control gain K^+ in the sequence; if it is, then the controller switches to this reference and control gain:

$$X(t) \in C(r^+, K^+, \rho^*(r^+, K^+, z)) \rightarrow r(t) = r^+, \; K(t) = K^+. \tag{20}$$

3.9 Cost Matrices

As described in the previous section, the connectivity graph matrix is comprised of ones and zeros, and thus, graph search results in a minimum length path between desired $r_i, r_j \in \mathcal{N}$.

In order to produce time efficient and thrust efficient paths, offline we simulate transitions between all $r_i, r_j \in \mathcal{N}$ for each $K \in \mathcal{K}$ and record the time and fuel consumption to reach a box of 1m around the target vertex. The results are merged into time and fuel matrices that store the respective minimum value, while in parallel, the control selectivity matrix identifies which gain K produced said minimum.

Step 3 in the motion planning procedure is augmented so that the graph connectivity matrix is multiplied elementwise with a desired cost matrix. Vertices that are not connected retain a corresponding matrix element of zero, while vertices that are connected now contain a matrix element of time or fuel cost.

3.10 Moving Debris Avoidance Approach

To avoid a non-stationary debris, its path can be covered by a union of a finite number of ellipsoidal sets,

$$\mathcal{D} = \bigcup_{l=1}^{l=n_d} O(z_l, Q_l), \tag{21}$$

where the center of the lth set is denoted by $z_l \in R^3$, and the lth set shape is defined by $Q_l = Q_l^{\mathrm{T}} > 0$. Then, the debris avoidance condition for the closed-loop trajectory that emanates from $X(0)$ with

the set-point r_i and gain K_j is given by

$$X(0) \in C(r_i, K_j, \rho) \text{ and } O(z_l, Q_l) \cap C(r_i, K_j, \rho) = \emptyset, \quad \text{for all } l = 1, \cdots, n_d. \tag{22}$$

The same approach, with larger n_d, can be used to handle *multiple* non-stationary debris. Note, however, that this approach is conservative as it does not account for the debris progressions along their paths versus time.

Hence, we introduce the notion of time into the problem; whereas a transition between r_i and r_j might not be feasible at time t_1, based on the motion of a debris, it might become feasible at time t_2. To accommodate moving debris, we introduce sets $C_k(r, K, \rho)$, $0 \leq k \leq N$, defined by the following relation,

$$\bar{A}(K)^k \Big(C_k(r, K, \rho) - \{X_e(r)\} \Big) \subseteq \Big(C(r, K, \rho) - \{X_e(r)\} \Big), \tag{23}$$

Note that if $X(0) \in C_k(r, K, \rho)$, then $X(1) \in C_{k-1}(r, K, \rho)$, $X(2) \in C_{k-2}(r, K, \rho), \cdots, X(k) \in C_0(r, K, \rho) = C(r, K, \rho)$. The set $C_k(r, K, \rho)$ can be much larger than $C(r, K, \rho)$; any states in $C_k(r, K, \rho)$ contract to $C(r, K, \rho)$ in k steps.

We now define *connectivity* between two vertices of the virtual net, $r_i \in \mathcal{N}$ and $r_j \in \mathcal{N}$ at a specified time t_0. This notion is based on the fact that the time to transition from any state in $C_N(r, K, \rho)$ to $C(r, K, \rho)$ is less or equal than N steps. Suppose that the debris path $D(t_0 : t_0 + N \cdot H)$ has been predicted over the $N \cdot H$ discrete steps from the time instant t_0, where

$$D(t_k : t_r) = \bigcup_{t=t_k}^{t=t_r} O(z(t), Q(t)).$$

The node $r_i \in \mathcal{N}$ is connected to $r_i \in \mathcal{N}$ at the time instant $t_k = t_0 + kN$ if there exists $K \in \mathcal{K}$ such that

$$D(t_k : t_k + N) \cap C(r_i, K, \rho) = \emptyset. \tag{24}$$

The node $r_i \in \mathcal{N}$ is connected to node $r_j \in \mathcal{N}$ at time t_k if there exists $K \in \mathcal{K}$ such that

$$D(t_k : t_k + N) \cap C_N(r_j, K, \rho) = \emptyset \tag{25}$$

and

$$C(r_i, K, \rho) \subset C_N(r_j, K, \rho). \tag{26}$$

The connectivity implies that a spacecraft located close to an equilibrium corresponding to r_i, $X_e(r_i)$, can transition close to an equilibrium $X_e(r_j)$ between the time instants t_k and $t_k + N$ while avoiding collision with the debris. We note that if r_i is connected to r_j this does not imply that, in turn, r_j is connected to r_i. We also note that connectivity depends on the existence of an appropriate control gain from the set of gains $\mathcal{K}$ but does not need to hold for all gains. Furthermore,

since connectivity depends on the predicted motion of the debris, connectivity/non-connectivity can depend on time.

The on-line motion planning with debris avoidance is performed according to the following procedure:

Step 1: Determine the debris location, shape and predict the debris path $D(t_0 : t_0 + N \cdot H)$

Step 2: Construct graph connectivity matrices corresponding to $t_k, k = 0, 1, \cdots, H$. In the graph connectivity matrix, if two vertices, r_i and r_j, are not connected at t_k, the corresponding matrix element is zero; if they are connected the corresponding matrix element is 1. In parallel, build the control gain selectivity matrix, which identifies the index of the highest preference gain K for which r_i and r_j are connected. This gain will be applied if the edge connecting r_i and r_j is traversed.

Step 3: Perform graph search to determine a sequence $r[t_k] \in \mathcal{N}$ and control gains $K[k] \in \mathcal{K}$, $k = 1, \cdots, l_p$, such that $r[t_1]$ satisfies the initial constraints, $r[l_p]$ satisfies the final constraints, and the path length l_p (or another cost function such as the expected fuel consumption or expected maneuver time) is minimized.

Per the above algorithm, a graph search is utilized to determine the minimum number of equilibrium hops around a debris starting at t_0.

Remark 1: The condition (25) is conservative. It can be replaced by a less conservative condition,

$$D(t_k : t_k + m) \cap C_{N-m}(r_j, K, \rho) = \{\emptyset\},$$
$$m = 0, 1, \cdots, N,$$

at a price of more demanding computations.

Remark 2: The condition (25) is checked computationally using the fast growth distance algorithm described in Section 3.7. The intersection is empty if C_N can be grown before it touches $D(t_k : t_k + N)$. This fast growth distance algorithm is essential to be able to rapidly construct the connectivity matrices.

Remark 3: In our simulations, the path search is performed using the standard Dijkstra's algorithm. It is applied to a lifted graph with vertices being the pairs (r_i, t_k).

3.11 Bounded Disturbances

We now discuss how the debris avoidance approach can be extended to handle bounded disturbances. For simplicity, we consider the case of multiple stationary debris. Consider the system

$$X_{k+1} = AX_k + BU_k + Bw, \tag{27}$$

where $w \in W$, W is the convex hull of w^i for $i = 1, \ldots, n_w$, w^i are the vertices of a disturbance set, and n_w is the number of vertices. Note that W is a compact set.

The positive invariance of $C(r,K,\gamma)$, $\gamma > 0$, for $W = \{0\}$ has already been established. When $W \neq \{0\}$, it can be shown that there exists $\gamma_{\min}$ such that the set is positively invariant for $\gamma > \gamma_{\min}$. Note that $\gamma_{\min} = \gamma_{\min}(K)$.

Since $C(r,K,\gamma_{\min}(K))$ is disturbance invariant, it contains the minimum invariant set that is an attractor for closed-loop trajectories, as long as r and K are maintained at constant values. Hence, in the case of bounded disturbances, connectivity can be redefined by replacing $X_e(r_i)$ in (19) with $C(r_i,K,\gamma_{\min}(K))$. Specifically, the vertex $r_i \in \mathcal{N}$ is connected to the vertex $r_j \in \mathcal{N}$ if there exists $K \in \mathcal{K}$ such that

$$C(r_i,K,\gamma_{\min}(K)) \subset int\, C(r_j,K,\rho^*(r_j,K,z)), \quad \text{for all } l = 1,\ldots,m. \tag{28}$$

The condition (28) ensures that a switch from r_i to r_j may occur and that subsequent dynamics will not lead to collision with the debris once $X(t) \in C(r_i,K,\gamma_{\min}(K))$.

To compute $\gamma_{\min}$ under all possible $w \in W$, it is sufficient to examine the flow at the vertices w^i of the disturbance set and demonstrate that if $X_k \in C(r,K,\gamma(K))$ and $w \in \{w^i, i = 1,\ldots,n_w\}$, then $X_{k+1} \in C(r,K,\gamma(K))$. The value $\gamma_{\min}$ is the minimum γ for which this condition holds.

To find $\gamma_{\min}$ we use a bilevel optimization strategy where the inner loop solves n_w optimization problems numerically with respect to X,

$$\begin{aligned} &\text{maximize} \quad F_i(X) = \tfrac{1}{2}(AX+BU+Bw^i)^{\mathrm{T}}\frac{P(K)}{\gamma_i^2}(AX+BU+Bw^i), \\ &\text{subject to} \quad \tfrac{1}{2}(X-X_e(r))^T P(K)(X-X_e(r)) \leq \gamma_i^2, \end{aligned} \tag{29}$$

and the outer loop performs bisections on each γ_i, so that all $F_i(X^*(\gamma_i))$, where $X^*(\gamma_i)$ denotes the inner-loop solution, are driven to 1. Thus, $\gamma_{\min} = \min(\gamma_i)$ for $i = 1,\ldots,n_w$. Note that $\gamma_{\min}$ is independent of equilibrium r, and so this calculation may be done once offline for each $K \in \mathcal{K}$ and stored onboard for real time implementation.

4 RESULTS AND DISCUSSION

Simulations are now provided that illustrate the debris avoidance approach. We consider a nominal circular orbit of 850 km and discretize the HCW equations with a sampling period, ΔT, of 30 seconds. We construct an approximately 2 km cubed virtual net. We let $\mathcal{K} = \{K_1, K_2, K_3\}$, where K_1, K_2, K_3 are the LQ gains associated with weight matrices $Q = \mathrm{diag}(100, 100, 100, 10^7, 10^7, 10^7)$, and $R_1 = 2\times10^5 I_3$, $R_2 = 2\times10^7 I_3$, and $R_3 = 2\times10^9 I_3$. These gains are chosen to represent preferences for fuel considerations, maneuver time considerations, and a compromise between them. We impose a maximum thrust constraint of 10 N in each axis. In all simulations, Dijkstra's algorithm is used to find the shortest cost path from initial node to final node.

4.1 Static Debris

We consider an ellipsoidal set $O(z_1, Q_1)$ over-bounding a debris centered at $z_1 = [0.3\ 0.4\ 0.5]^{\mathrm{T}}$ km, where $Q_1 = 100I_3$. We use the technique of [25] where bisections are applied to (11) to determine the growth distance to the debris from each node in the net. The spacecraft's initial condition is $X(0) = X_e(r_0)$, where $r_0 = [0.32\ 0\ 1.61]^{\mathrm{T}}$ km. The target equilibrium node is $X_e(0)$.

Figure 4 shows the path the spacecraft takes under closed-loop control in order to avoid the debris. The green x marks the initial node. The blue x marks the final node. The red ellipsoid represents the debris. The blue line is the path the spacecraft takes in order to avoid the debris. The blue ellipsoids represent the invariant sets along the path. The spacecraft is able to complete the desired maneuver well within maximum thrust constraints while successfully avoiding the debris. In Figure 5 we rerun the simulation for a grid of initial conditions. The figure clearly demonstrates the initial conditions for which the maneuver path is perturbed from that which the spacecraft would have taken had there been no debris.

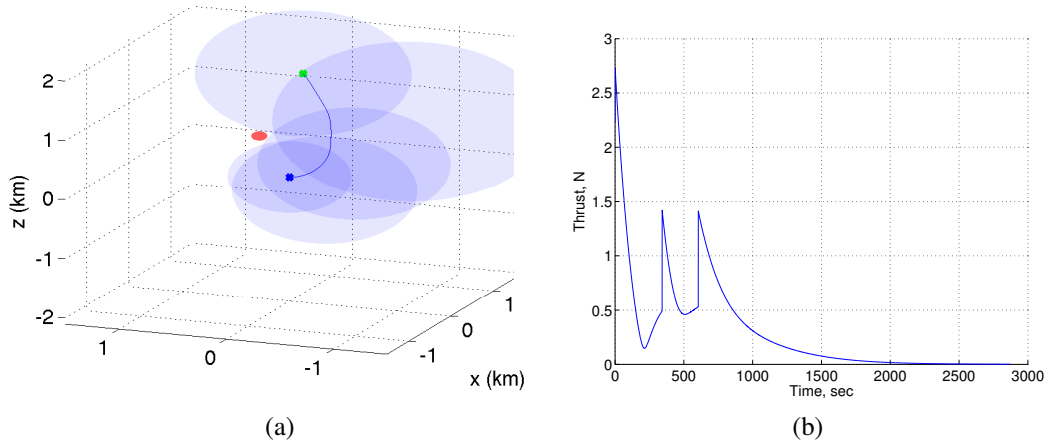

(a) (b)

Figure 4: (a) Debris avoidance path for a single debris. (b) The time history of thrust magnitude.

Next, we add a second debris $O(z_2, Q_2)$ centered at $z_2 = [0.3\ -0.4\ 0.5]^{\mathrm{T}}$, where $Q_2 = 100I_3$. In calculating the growth distance, we take the minimum distance to each of $O(z_i, Q_i)$, $i = 1, 2$. Figure 6 shows the path the spacecraft takes under closed-loop control in order to avoid both debris.

4.2 Moving Debris

We consider the case of a non-stationary debris where we treat its motion as the union of static debris along the path (21). A union of ellipsoidal sets over-bounds the debris' motion, where the debris positions z_i are generated by sampling the relative motion of the debris with the initial condition $[0\ 0.5\ 0\ 0\ 0.0006\ 0]^{\mathrm{T}}$, and where $Q_i = 200I_3, i = 1 \ldots n_d$. The spacecraft's initial condition is $X(0) = X_e(r_0)$, where $r_0 = [0\ 1\ 0]^{\mathrm{T}}$ km. The target equilibrium node is $X_e(r_d)$, where $r_0 = [0\ -$

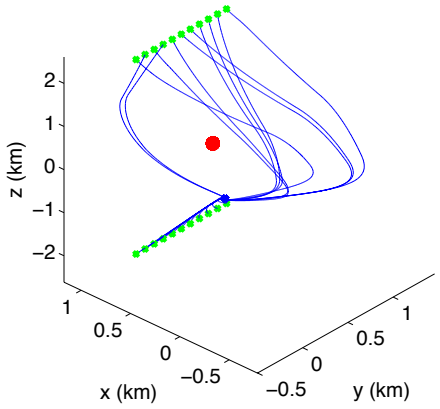

Figure 5: Debris avoidance paths for many initial conditions. Each green x marks an intial condition. We do not show the invariant set ellipsoids for visual clarity.

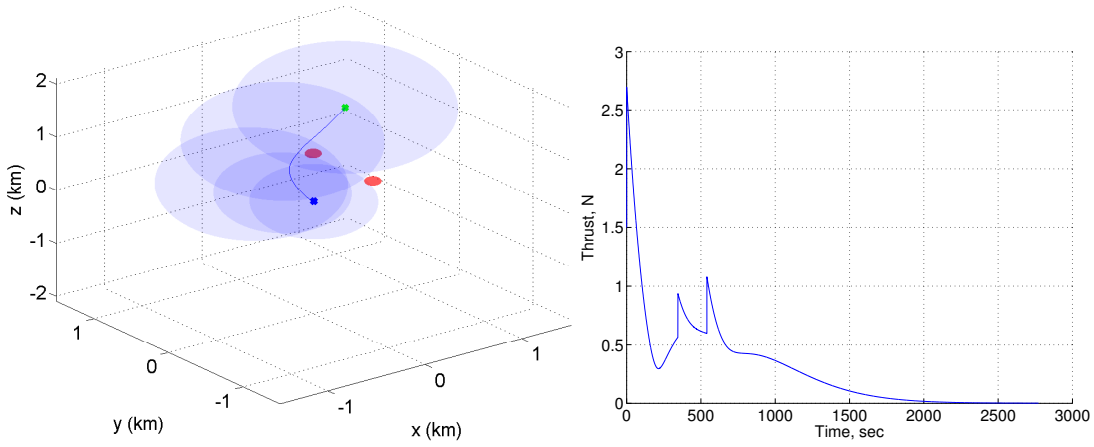

(a) (b)

Figure 6: (a) Debris avoidance path for 2 pieces of debris. (b) The time history of thrust magnitude.

$1\ 0]^{\mathrm{T}}$ km. We use the single gain K_2 and do not include fuel or time cost matrices in the simulation, searching for a minimum length path. Figure 7 demonstrates that the spacecraft is able to avoid the closed debris path by 'hopping' under it. The green x marks the initial node. The blue x marks the final node. The red ellipsoids represent the debris path. The blue line is the path the spacecraft takes in order to avoid the debris. The blue ellipsoids represent the maximally grown invariant sets, C, along the path.

In Figure 8, we repeat the simulation for time efficient and thrust efficient paths and allow all $K \in \mathcal{K}$. Table 1 summarizes the total time, thrust and nodes traversed for the three paths. Note that the minimum length path now 'hops' over the debris path instead of under it, as now that it has access to K_1 it finds a shorter path. Also note that the time efficient path takes longer to complete than the minimum length path. While the cost matrices described in Section 3.9 calculate time and thrust to travel between all vertices in the virtual net, the execution of the path does not require the spacecraft to reach intermediate vertices, rather, switching to the next reference once the current state enters the next reference's invariant set (20). As such, the cost matrices only provide a heuristic for selecting efficient paths. In Figure 9 we require the paths to travel through intermediate vertices to show that, in this case, the cost matrices accurately determine efficient paths. The results are summarized in Table 2.

Table 1: Total Time, Thrust, and Nodes Traversed for all Maneuver Paths for a Union of Static Debris.

	Total Time	Total Thrust	Total # of Nodes	Gains used
Minimum Length Path	2611.5 s	1472.85 N·s	6	K_1
Time Efficient Path	2841 s	1264.95 N·s	6	K_1, K_2
Thrust Efficient Path	9177 s	671.297 N·s	11	K_2, K_3

Table 2: Total Time, Thrust, and Nodes Traversed for all Maneuver Paths that Travel Through Intermediate Nodes for a Union of Static Debris.

	Total Time	Total Thrust	Total # of Nodes	Gains used
Minimum Length Path	10457.5 s	3006.13 N·s	6	K_1
Time Efficient Path	9862 s	2017.11 N·s	6	K_1, K_2
Thrust Efficient Path	32812.5 s	1083.58 N·s	11	K_2, K_3

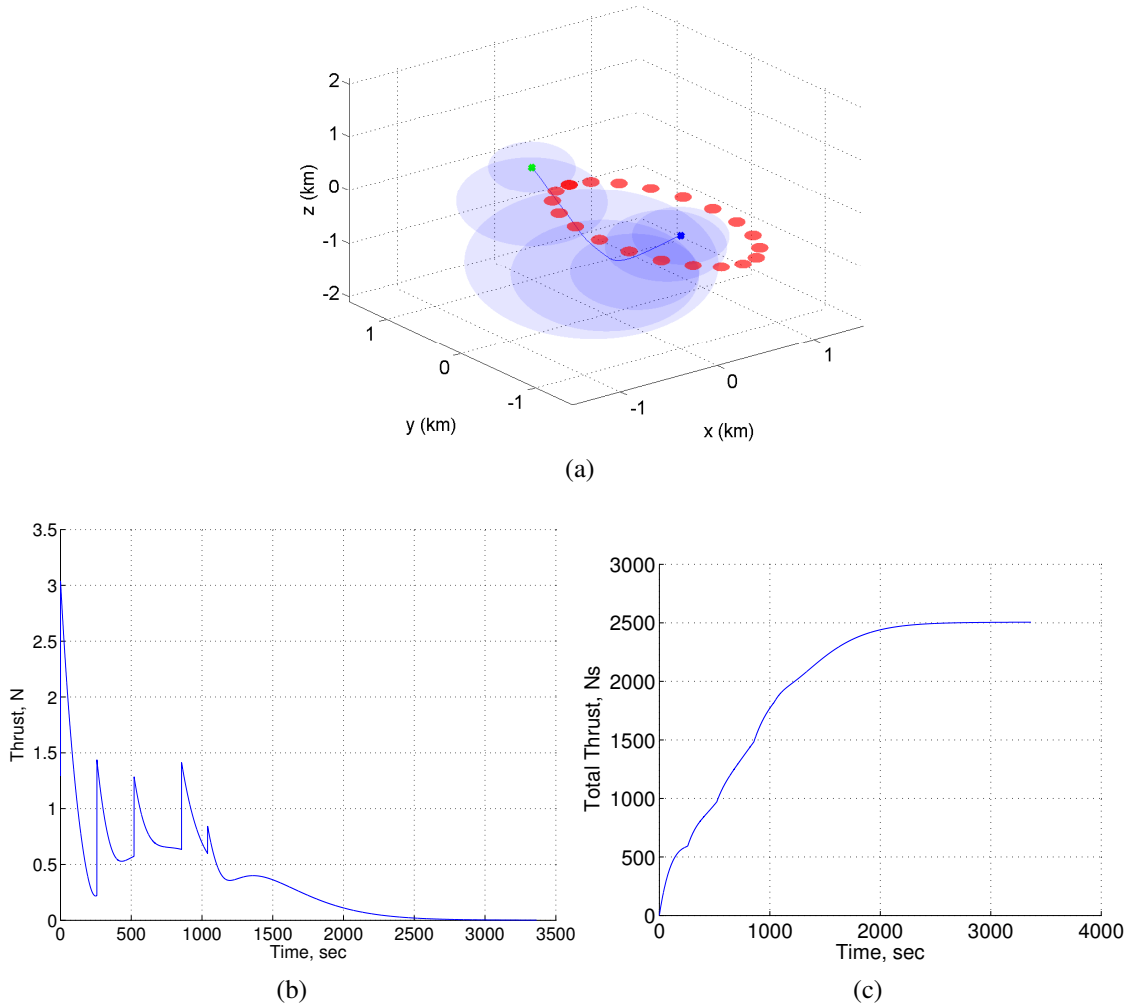

(a)

(b)

(c)

Figure 7: (a) Debris avoidance path for a non-stationary debris using the union method. (b) The time history of thrust magnitude. (c) Cumulative thrust vs time.

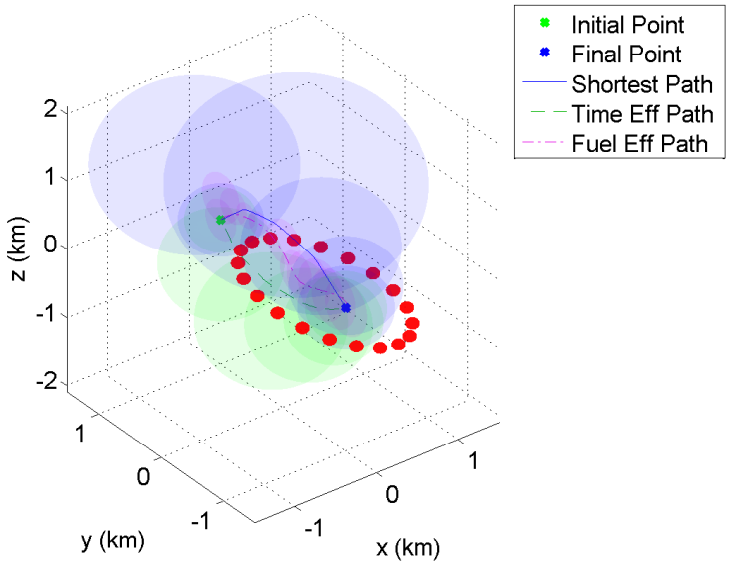

(a)

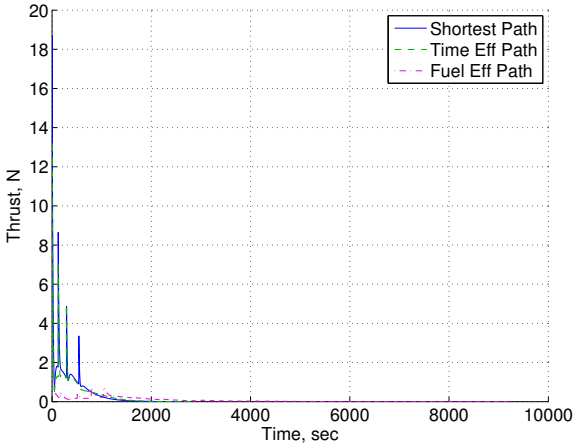

(b)

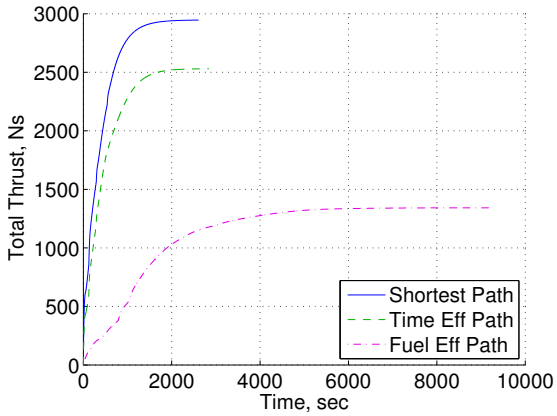

(c)

Figure 8: (a) Multiple debris avoidance paths for a non-stationary debris using the union method. (b) The time history of thrust magnitude. (c) Cumulative thrust vs time.

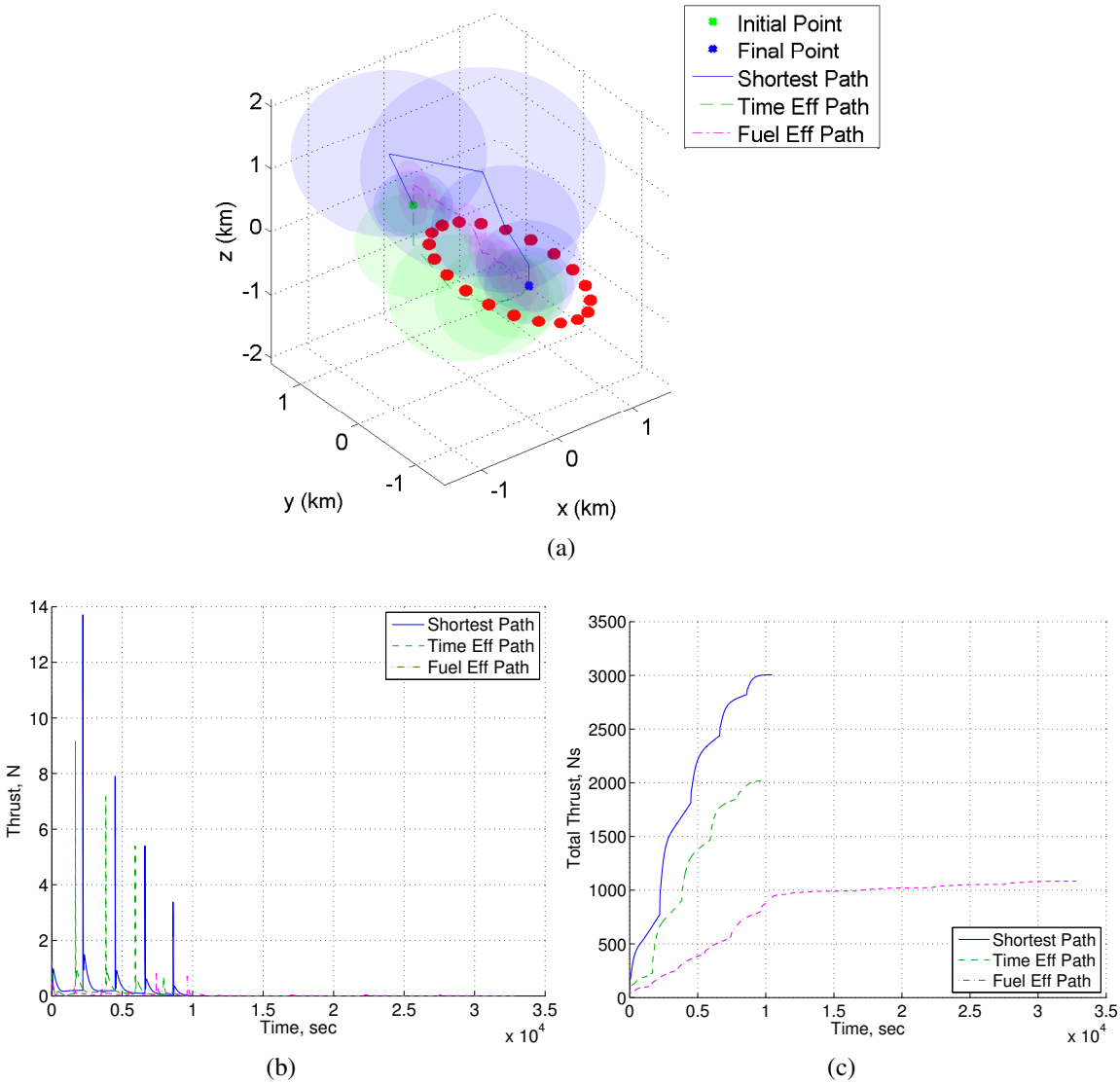

Figure 9: (a) Debris avoidance paths that travel via intermediate nodes for a non-stationary debris using the union method. (b) The time history of thrust magnitude. (c) Cumulative thrust vs time.

We now repeat the simulations taking into account the debris' motion as a function of time. We use the single gain K_2 and do not include fuel or time cost matrices in the simulation, searching for a minimum length path. Figure 10 shows that the graph search algorithm is able to find a path which passes through the debris' path but avoids collision due to the debris' location elsewhere at the specific time instant at which the spacecraft path crosses the debris' path. In Figure 11, we repeat the simulation for a thrust efficient path. Table 3 summarizes the total time, thrust and nodes traversed for the two paths. Note that the thrust efficient path uses more thrust than the minimum length path. In Figure 12 we require the paths to travel through intermediate vertices to show that, in this case, the thrust cost matrix accurately determines an efficient path. The results are summarized in Table 4.

Table 3: Total Time, Thrust, and Nodes Traversed for all Maneuver Paths using the Contractive Set Approach.

	Total Time	Total Thrust	Total # of Nodes
Minimum Length Path	4635.5 s	4635.5 N·s	7
Thrust Efficient Path	4703.5 s	781.407 N·s	7

Table 4: Total Time, Thrust, and Nodes Traversed for all Maneuver Paths that Travel Through Intermediate Nodes using the Contractive Set Approach.

	Total Time	Total Thrust	Total # of Nodes
Minimum Length Path	13388.5 s	2060.14 N·s	7
Thrust Efficient Path	12657.5 s	957.116 N·s	7

Finally, we run the simulation for the case of bounded disturbances. We consider $W = \{w : \|w\|_\infty \leq \varepsilon\}$ for which $n_w = 8$, that is, disturbances that fit in a box of magnitude ε. In Figure 13 we consider a uniform distribution of disturbances, for $\varepsilon = 0.1$ N and $\varepsilon = 0.2$ N. The orange ellipsoids represent the disturbance invariant sets $C(r, K, \gamma_{\min}(K))$, along the path. The spacecraft is able to safely avoid the debris' path despite being subjected to disturbances.

5 CONCLUSIONS

We described a technique for spacecraft maneuver planning that uses positively-invariant sets in order to avoid collisions with debris, while adhering to specified thrust limits. The approach is based on hopping between neighborhoods of equilibria in a virtual net, and maintaining the spacecraft trajectory within a tube formed by safe positively-invariant sets. For the case where thrust limits can be specified as polyhedral norm bounds, we have shown that the thrust limit on the growth distance can be easily computed; it is, in fact, feasible to perform these computations onboard a

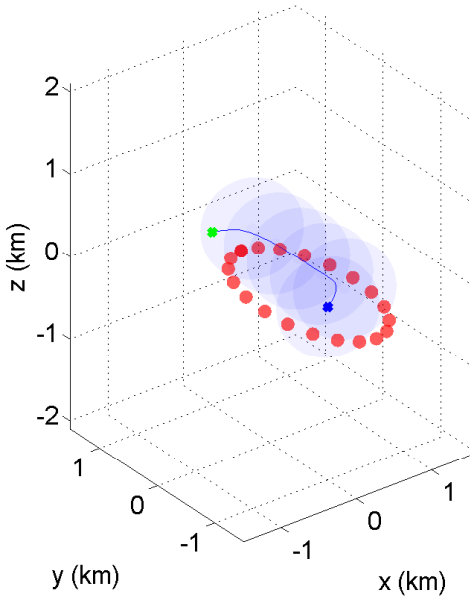

(a)

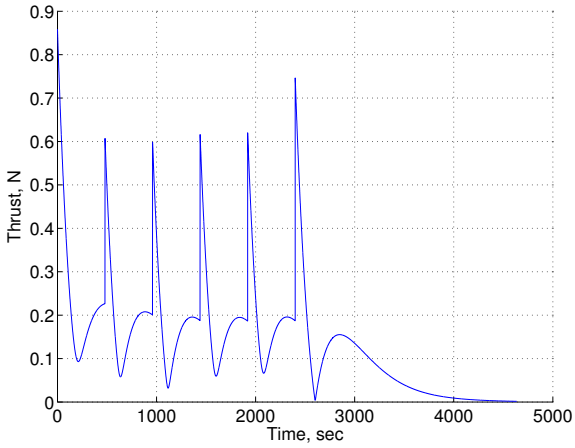

(b)

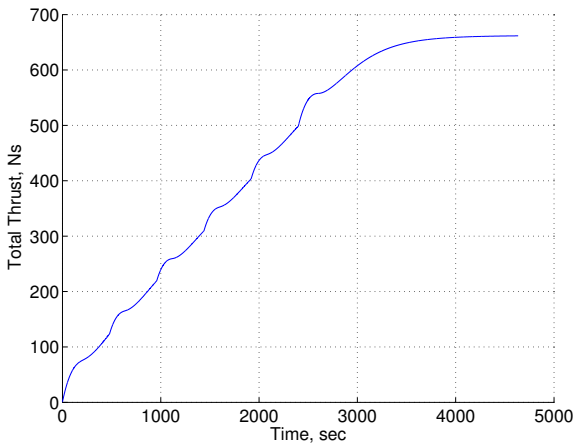

(c)

Figure 10: (a) Debris avoidance path for a non-stationary debris using the contractive set approach. (b) The time history of thrust magnitude. (c) Cumulative thrust vs time.

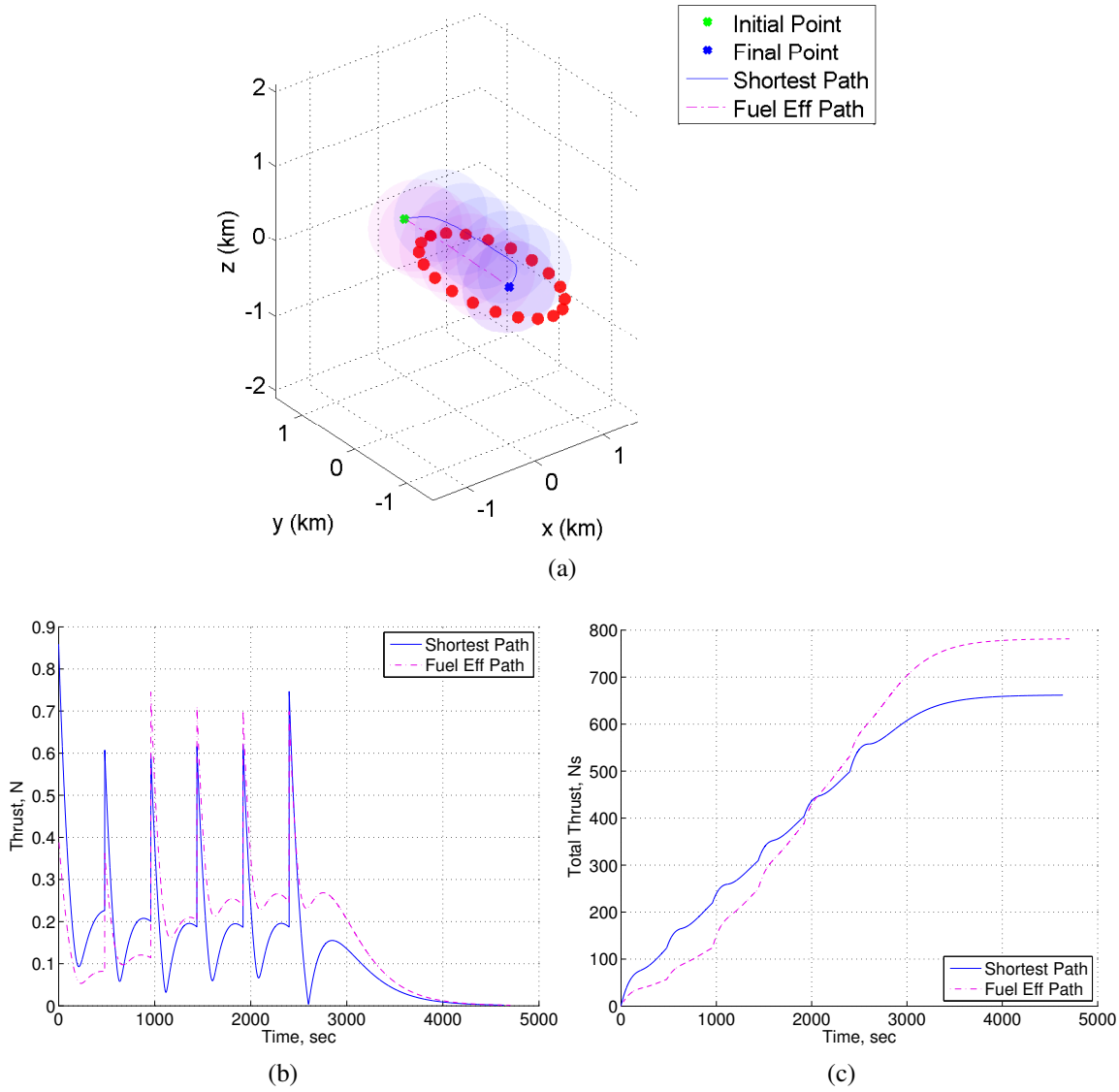

Figure 11: (a) Multiple debris avoidance paths for a non-stationary debris using the contractive set approach. (b) The time history of thrust magnitude. (c) Cumulative thrust vs time.

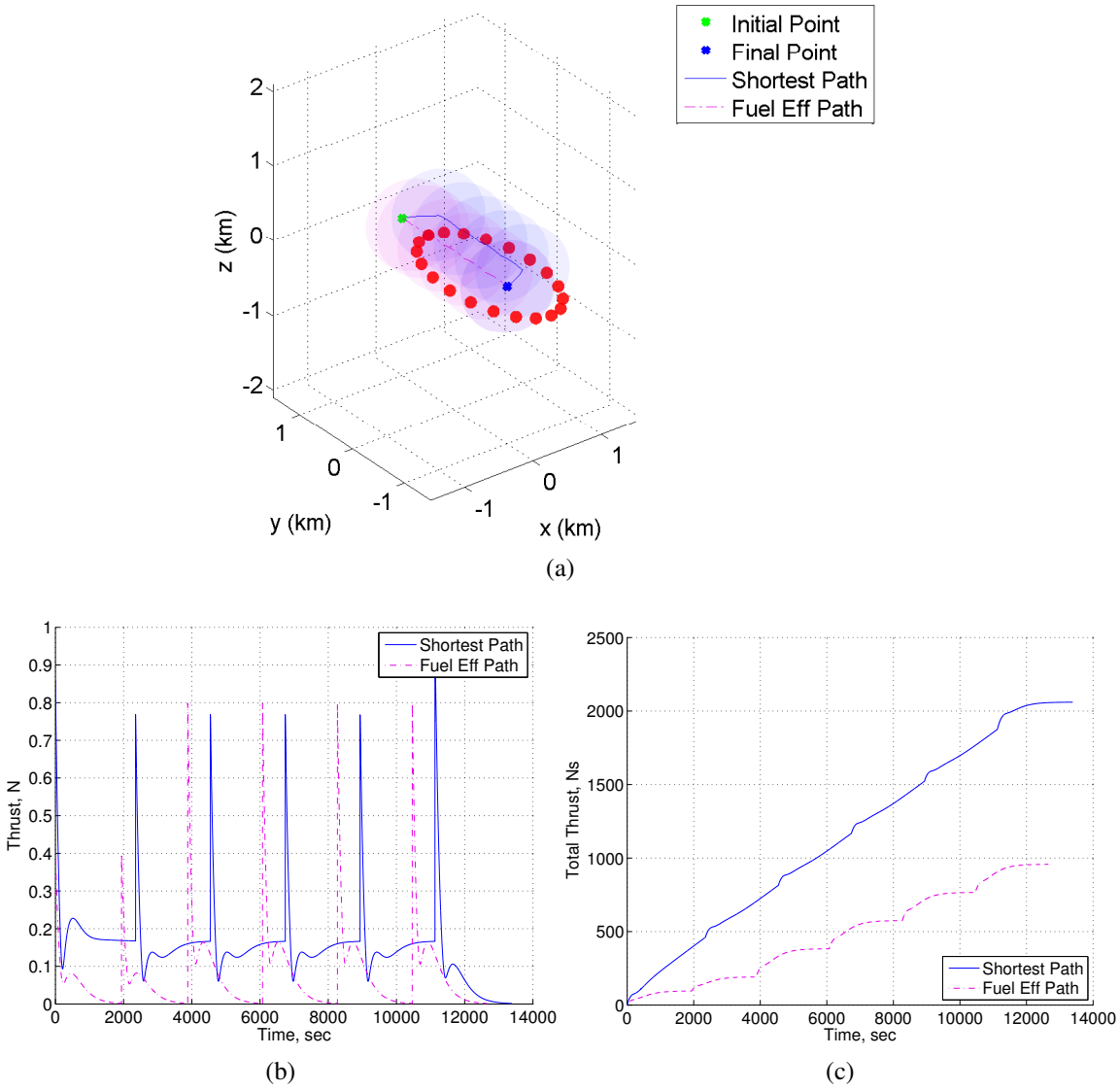

Figure 12: (a) Debris avoidance paths that travel via intermediate nodes for a non-stationary debris using the contractive set approach. (b) The time history of thrust magnitude. (c) Cumulative thrust vs time.

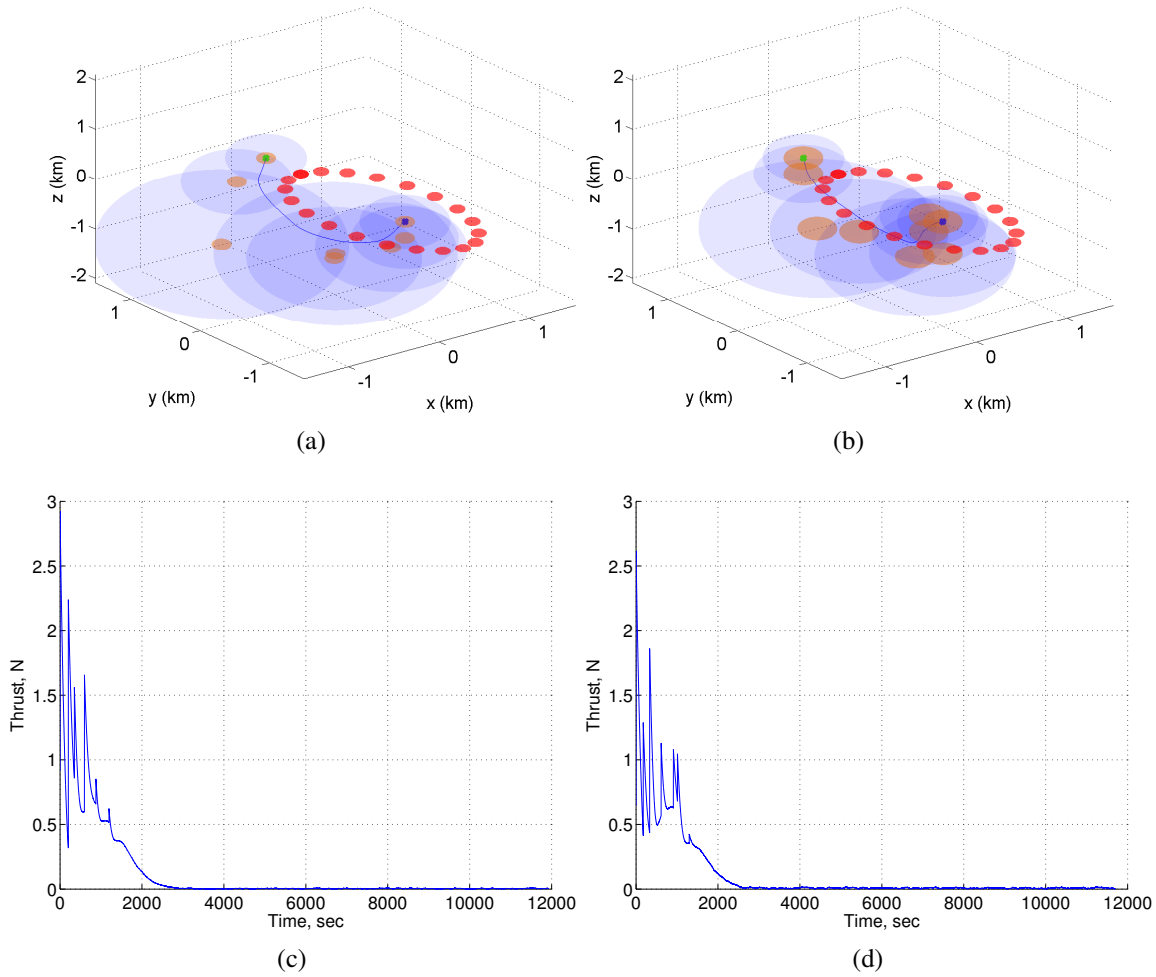

Figure 13: (a) Debris avoidance path for a non-stationary debris under uniform random disturbance with $\varepsilon = 0.1$ N. (b) $\varepsilon = 0.2$ N. (c), (d) Time histories of thrust magnitude.

spacecraft in order to account for thruster failure or degradation. We described an extension in the presence of moving debris using contractive constraint admissible sets in order to avoid collisions. Lastly, we illustrated that the approach can be extended to include unmeasured bounded disturbances.

Future Work

Developing cost matrices that accurately capture the cost of maneuvers that do not travel through intermediate nodes is a topic for future investigation.

The constraint-admissible positively invariant set method can be extended to attitude control on SO(3) that is capable of handling inequality constraints associated with control authority limits and conical keep-out zones. The controller would use a supervisory strategy with an inner-loop Lyapunov SO(3)-based controller, such as the inertia-free controllers presented in this work, and an outer loop set-point guidance based on positively invariant constraint admissible sets with real-time graph search. The combined methodology would reduce the search space of possible attitude maneuver solutions and effectively handle constraints.

Future work will also consider ways to apply the safe positively invariant set method to non-spacecraft problems, such as ground and other autonomous vehicles.

REFERENCES

[1] Kolmanovsky, I. and Gilbert, E., "Theory and computation of disturbance invariant sets for discrete-time linear systems," *Mathematical Problems in Engineering*, Vol. 4, No. 4, 1998, pp. 317–367.

[2] Wie, B., *Spacecraft Dynamics and Control*, AIAA, Reston, VA, 2nd ed., 2010.

[3] for the Assessment of NASA's Orbital Debris Programs; National Research Council, C., *Limiting Future Collision Risk to Spacecraft:An Assessment of NASA's Meteoroid and Orbital Debris Programs*, The National Academies Press, 2011.

[4] LaValle, S. M., *Planning Algorithms*, Cambridge University Press, 1996.

[5] Maia, M. H. and Galvao, R. K. H., "On the use of mixed-integer linear predictive control with avoidance constraints," *International Journal of Robust and Nonlinear Control*, Vol. 19, 2008, pp. 822–828.

[6] Ranieri, C., "Path-Constrained Trajectory Optimization for Proximity Operations," *AIAA/AAS Astrodynamics Specialist Conference*, Honolulu, HI, August 2008.

[7] Betts, J. T. and Huffman, W. P., "Sparse optimal control software SOCS," *Mathematics and Engineering Analysis Technical Document MEA-LR-085,* Boeing Information and Support Services, The Boeing Company, Seattle, WA, July 1997.

[8] Epenoy, R., "Fuel optimization for continuous-thrust orbital rendezvous with collision avoidance constraint," *Journal of Guidance, Control, and Dynamics*, Vol. 34, No. 2, 2011.

[9] Martinson, N., "Obstacle avoidance guidance and control algorithms for spacecraft maneuvers,"," *Proceedings of AIAA Guidance, Navigation, and Control Conference*, Chicago, IL, August 2009.

[10] Sanchez-Ortiz, N., Bello-Mora, M., and Klinkrad, H., "Collision avoidance manoeuvres during spacecraft mission lifetime: Risk reduction and required Δ V," *Advances in Space Research*, Vol. 38, 2006.

[11] Martinson, N., Munoz, J., and Wiens, G., "A new method of guidance control for autonomous rendezvous in a cluttered space environment," *Proceedings of AIAA Guidance, Navigation, and Control Conference*, Hilton Head, SC, August 2007.

[12] Mueller, J. B., Griesemer, P. R., and Thomas, S., "Avoidance maneuver planning incorporating station-keeping constraints and automatic relaxation," *AIAA Infotech@Aerospace 2010*, Atlanta, GA, April 2010.

[13] Ulybyshev, Y., "Trajectory optimization for spacecraft proximity operations with constraints," *AIAA Guidance, Navigation, and Control Conference*, Portland, OR, August 2011.

[14] Richards, A., Schouwenaars, T., How, J., and Feron, E., "Spacecraft trajectory planning with avoidance constraints using mixed-integer linear programming," *AIAA Journal of Guidance, Control, and Dynamics*, Vol. 25, No. 4, August 2002.

[15] Mueller, J. B., "Onboard planning of collision avoidance maneuvers using robust optimization," *AIAA Infotech@ Aerospace Conference, Seattle, AIAA, Washington, DC*, Seattle, WA, April 2009.

[16] Kolmanovsky, I. and Gilbert, E., "Multimode regulators for systems with state and control constraints and disturbance inputs," *Proceedings of Workshop Control Using Logic-Based Switching*, edited by M. A.S, Springer-Verlag, Block Island, Rhode Island, 1997, pp. 104–117.

[17] Blanchini, F. and Miani, S., *Set-theoretic methods in control*, Birkhäuser Boston, 2007.

[18] Blanchini, F., "Set invariance in control," *Automatica*, Vol. 35, No. 11, 1999, pp. 1747–1767.

[19] Park, H., Di Cairano, S., and Kolmanovsky, I., "Linear Quadratic Model Predictive Control approach to spacecraft rendezvous and docking," *Proceedings of 21st AAS/AIAA Space Flight Mechanics Meeting*, New Orleans, Louisiana, USA, 2011, pp. Paper AAS–142.

[20] Ong, C. J. and Gilbert, E. G., "Growth distances: New measures for object separation and penetration," *IEEE Transactions on Robotics and Automation*, Vol. 12, No. 6, 1996, pp. 888–903.

[21] Luenberger, D. G. and Ye, Y., *Linear and nonlinear programming*, Vol. 116, Springer, 2008.

[22] Bazaraa, M. S., Sherali, H. D., and Shetty, C. M., *Nonlinear programming: theory and algorithms*, Wiley-interscience, 2006.

[23] Guddat, J., Vazquez, F. G., and Jongen, H. T., *Parametric optimization: singularities, path-following and jumps*, Teubner, 1990.

[24] Quoc, T. D., Savorgnan, C., and Diehl, M., "Adjoint-based predictor-corrector sequential convex programming for parametric nonlinear optimization," *SIAM Journal on Optimization*, Vol. 22, No. 4, 2012, pp. 1258–1284.

[25] Baldwin, M., Weiss, A., Kolmanovsky, I., and Erwin, R. S., "Spacecraft Debris Avoidance using Constraint Admissible Positively Invariant Sets," *Proceedings of AAS Space Flight Mechanics Meeting*, Charleston, South Carolina, 2012, pp. Paper AAS 12–250.

[26] Curtis, H. D., *Orbital mechanics for engineering students*, Butterworth-Heinemann, 2005.

[27] Fehse, W., *Automated Rendezvous and Docking of Spacecraft*, Cambridge Aerospace Series, 2003.

APPENDIX

This appendix provides the necessary background on spacecraft relative motion orbital dynamics.

A.1 Spacecraft Relative Motion Orbital Dynamics

In traditional relative motion problems, an approaching spacecraft is maneuvered close to a target spacecraft in a nominal orbit. The target spacecraft is assumed to be at the origin of Hill's frame. See Fig A.1.

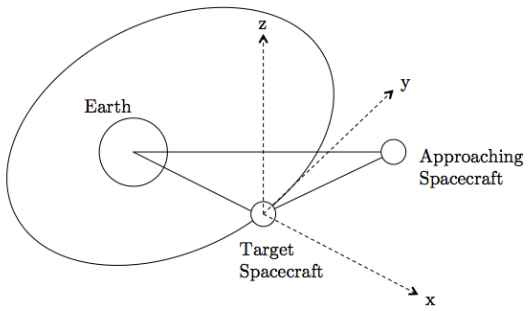

Figure A.1: Hill's frame.

A.1.1 Nonlinear equations of motion

The relative position vector of the spacecraft with respect to a target location on an orbit is expressed as

$$\delta\vec{r} = x\hat{i} + y\hat{j} + z\hat{k},$$

where x, y and z are the components of the position vector of the spacecraft relative to the target location and $\hat{i}$, $\hat{j}$, $\hat{k}$ are the unit vectors of the Hill's frame. The Hill's frame has its x-axis along the orbital radius, y-axis orthogonal to the x-axis and in the orbital plane, and z-axis orthogonal to orbital plane.

The position vector of the spacecraft with respect to the center of the Earth is given by $\vec{R} = \vec{R}_0 + \delta\vec{r}$, where $\vec{R}_0$ is the nominal orbital position vector. The nonlinear equation of motion for the spacecraft (relative to an inertial frame) is given by

$$\ddot{\vec{R}} = -\mu\frac{\vec{R}}{R^3} + \frac{1}{m_c}\vec{F}, \tag{A.1}$$

where $\vec{F}$ is the vector of external forces applied to the spacecraft, $R = |\vec{R}|$, m_c is the mass of the spacecraft, and μ is the gravitational constant.

A.1.2 Linearized equations on circular orbits

For $\delta r << R$, the linearized CWH equations [2] approximate the relative motion of the spacecraft on a circular orbit as

$$\begin{aligned} \ddot{x} - 3n^2 x - 2n\dot{y} &= \frac{F_x}{m_c}, \\ \ddot{y} + 2n\dot{x} &= \frac{F_y}{m_c}, \\ \ddot{z} + n^2 z &= \frac{F_z}{m_c}, \end{aligned} \tag{A.2}$$

where F_x, F_y, F_z are components of the external force vector (excluding gravity) acting on the spacecraft, and $n = \sqrt{\frac{\mu}{R_0^3}}$ denotes the mean motion of the nominal orbit. The linearized dynamics account for differences in gravity between the spacecraft and nominal orbital location, and for relative motion effects. The spacecraft relative motion dynamics in the orbital plane (x and y) and in the out-of-orbital plane (z) are decoupled. The in-plane dynamics are Lyapunov unstable (2 eigenvalues at the origin and 2 eigenvalues on the imaginary axis at n), while the out-of-plane dynamics are Lyapunov stable (2 eigenvalues on the imaginary axis at n). The in-plane dynamics are completely controllable from F_y input but are not controllable from F_x input. The out-of-plane dynamics are controllable from F_z input.

Assuming a sampling period of ΔT sec, we can convert the model (A.2) to a discrete-time form

$$X_{k+1} = AX_k + BU_k, \tag{A.3}$$

where $X_k = [x_k,\ y_k,\ z_k,\ \dot{x}_k,\ \dot{y}_k, \dot{z}_k]^{\mathrm{T}}$ is the state at time step $k \in Z^+$, $U_k = [F_{x,k},\ F_{y,k},\ F_{z,k}]^{\mathrm{T}}$ is the control vector of thrust forces at the time step $k \in Z^+$, and $A = \exp(A_c \Delta T)$, $B = \int_0^{\Delta T} \exp(A_c(\Delta T - \tau))d\tau B_c$ are the discretized matrices obtained based on the continuous-time system realization (A_c, B_c) in (A.2). Alternatively, the control vector U can represent an instantaneous change in the velocity of the spacecraft, Δv, induced by thrust, with an appropriately re-defined B-matrix,

$$B_{\Delta v} = e^{A_c \Delta T} \begin{bmatrix} 0 & 0 & 0 \\ 0 & 0 & 0 \\ 0 & 0 & 0 \\ 1 & 0 & 0 \\ 0 & 1 & 0 \\ 0 & 0 & 1 \end{bmatrix}.$$

A.1.3 Linearized equations on elliptic orbits

For generic elliptic orbits of arbitrary eccentricity, the linearization of these equations is described by linear time-varying equations [26],

$$\begin{aligned}
\frac{F_x}{m_c} &= \delta\ddot{x} - \left(\frac{2\mu}{R_0^3(t)} + \frac{h^2}{R_0^4(t)}\right)\delta x + \frac{2\left(v_0(t)\cdot R_0(t)\right)h}{R_0^4(t)}\delta y \\
&\quad - 2\frac{h}{R_0^2(t)}\delta\dot{y}, \\
\frac{F_y}{m_c} &= \delta\ddot{y} + \left(\frac{\mu}{R_0^3(t)} - \frac{h^2}{R_0^4(t)}\right)\delta y - \frac{2\left(v_0(t)\cdot R_0(t)\right)h}{R_0^4(t)}\delta x \\
&\quad + 2\frac{h}{R_0^2(t)}\delta\dot{x}, \\
\frac{F_z}{m_c} &= \delta\ddot{z} + \frac{\mu}{R_0^3(t)}\delta z,
\end{aligned} \tag{A.4}$$

where δx, δy and δz are (relative) coordinates of the spacecraft in Hill's frame, F_x, F_y, F_z are components of the external force vector (excluding gravity) acting on the spacecraft, h is the orbit angular momentum, $R_0(t)$ is the nominal time-varying orbital radius, and $v_0(t)$ is the nominal time-varying orbital velocity. Equation (A.2) assumes that the target spacecraft motion is in an ideal Keplerian orbit; if its motion is affected by perturbations, F_x, F_y, F_z have to be modified to account for these perturbations [27]. We assume that F_x, F_y, F_z are thrust forces that can be realized via on-board thruster on-off time allocation and attitude control system commands [27].

LIST OF SYMBOLS, ABBREVIATIONS, AND ACRONYMS

CWH Clohessy-Wiltshire-Hill

LTV linear time-varying

DISTRIBUTION LIST

DTIC/OCP
8725 John J. Kingman Rd, Suite 0944
Ft Belvoir, VA 22060-6218 1 cy

AFRL/RVIL
Kirtland AFB, NM 87117-5776 2 cys

Official Record Copy
AFRL/RVSV/Morgan Baldwin 1 cy

(This page intentionally left blank)